



Oscillatory phenomena in electrophysiological networks: The coupling between cell bioelectricity and transcription



Javier Cervera^{a,*}, José A. Manzanares^a, Michael Levin^{b,c,d}, Salvador Mafe^{a,c}

^a Dept. Termodinàmica, Facultat de Física, Universitat de València, 46100, Burjassot, Spain

^b Dept. of Biology, Tufts University, Medford, MA, 02155, USA

^c Allen Discovery Center at Tufts University, Medford, MA, 02155, USA

^d Wyss Institute for Biologically Inspired Engineering, Harvard University, Boston, MA, 02215, USA

ARTICLE INFO

Keywords:

Electrophysiological networks
Oscillatory phenomena
Bioelectricity
Transcription
Cell membrane potential

ABSTRACT

Morphogenetic regulation during embryogenesis and regeneration rely on information transfer and coordination between different regions. Here, we explore theoretically the coupling between bioelectrical and transcriptional oscillations at the individual cell and multicellular levels. The simulations, based on a set of ion channels and intercellular gap junctions, show that bioelectrical and transcriptional waves can electrophysiologically couple distant regions of a model network in phase and antiphase oscillatory states that include synchronization phenomena. In this way, different multicellular regionalizations can be encoded by cell potentials that oscillate between depolarized and polarized states, thus allowing a spatio-temporal coding. Because the electric potential patterns characteristic of development and regeneration are correlated with the spatial distributions of signaling ions and molecules, bioelectricity can act as a template for slow biochemical signals following a hierarchy of experimental times. In particular, bioelectrical gradients that couple cell potentials to transcription rates give to each single cell a rough idea of its location in the multicellular ensemble, thus controlling local differentiation processes that switch on and off crucial parts of the genome.

1. Introduction

Multicellular aggregates of interacting cells can coordinate individual transcriptional states through the spatio-temporal distribution of regulatory agents. The traditional systems-level view of signal integration in pattern dynamics and development [1–3] tends to emphasize biochemical signals and biomechanical fields in the modeling of transduction networks and collective gene-expression patterns [4–6]. The cells within an aggregate have the same genetic material and need an internal representation of their states [7] for spatio-temporal regionalization. The membrane potential, which reflects environmental conditions including the neighboring cell states, can also provide spatial information [6,8–13]. Experimentally, polarized and depolarized potential regions are clearly visible in tissues and model animals [8,9]. Also, oscillatory electrical potentials pervade a broad range of spatio-temporal scales of biological organization. Here we explore how bioelectrical networks could contribute to the spatio-temporal coordination of cells over long-distance regions, a crucial process in embryogenesis and regeneration [14–16]. While we have not attempted to model a

particular experimental system, our approach provides a conceptual scenario where regulatory feedbacks between cell bioelectricity and transcription contribute to the spatio-temporal integration of a multicellular aggregate.

The interplay between bioelectrical and biochemical signals have recently been emphasized [8–11,16–21]. Cell membrane potentials modulate transcription of numerous gene targets through transduction mechanisms related to biochemical downstream processes [18]. In particular, the cell potential regulates the local calcium concentration, which in turn influences transcription and proliferation. For instance, electro-genetic cell control can be achieved by coupling calcium levels to the expression of a set of counteracting voltage-gated channels that modulate intracellular calcium concentration through the cell potential [20]. In this way, pluripotency factors and differentiation programs can be influenced in critical stages of embryonic development [21]. Remarkably, this interplay is also observed in circadian rhythms and the cell cycle [22,23]. In a different but related context, ion channels and time-dependent membrane potentials are also central to bacterial communication [24,25].

* Corresponding author.

E-mail address: jcervera@uv.es (J. Cervera).

The *polarized* (high absolute value) and *depolarized* (low absolute value) cell membrane potentials allow to integrate single-cell states into multicellular states where the local electric potentials are transduced into different protein expressions in the long term [8,9,16]. The spatio-temporal multicellular patterns of bi-stable non-excitable cells show stationary and oscillatory cell potentials that are instructive for developmental, regenerative, and tumorigenesis processes (see Fig. S1 of *Supplementary Material*) because these patterns can reflect environmental and developmental conditions, in loose analogy of the fast-wave cell potentials of neural patterns that represent the outside world [8,26].

In our computational biology study, we explore the coupling between bioelectrical and biochemical oscillations at the individual cell and multicellular levels. This coupling is based on our previous model [16] and shows that two populations of spatially segregated cells with different bioelectrical properties can lead to oscillations between depolarized and polarized states in multicellular regions. These states allow a spatio-temporal coding for the different regions of the multicellular aggregate on the basis of their distinct polarization states. Because the electric potential patterns characteristic of developmental and regeneration stages are correlated with the spatial distributions of signaling ions and molecules, bioelectricity can act as a template for slow biochemical signals following a hierarchy of experimental times in morphological and developmental processes [27–29]. Note that rhythms in somatic tissues outside the brain and spinal cord are usually ascribed to the coding of biochemical oscillatory signals, being recognized as important in the storage and processing of global information [30–37]. In this context, hyperpolarizing and depolarizing events, bioelectrical rhythms, and oscillations can offer a complementary view because of the inclusion of cell potentials [19,28,38–42]. Also, the coupling between bioelectricity and transcription at the multicellular level provides an interesting addition to network science, which finds a variety of applications in different biological fields [43–45]. In this context, recent reviews have focused on network robustness and resilience [43], paying attention to the control of disruption amplification at the system-wide level, the different collective models of signal propagation [44], and the network implications of morphology and structural design in living systems [45].

2. Modeling of single-cell and multicellular bioelectrical states

It is important to note that our theoretical approach is *not a simple*

equivalent circuit model: the cell is characterized by the *interplay between genetic and bioelectric networks* at the single-cell scale, and this coupling is extended to the multicellular scale by the intercellular gap junctions [46]. Thus, the cell state is iterated with time in the simulations to encode the positional information at the multicellular scale and long-range temporal coordination of gene expression is then obtained.

For the sake of clarity, we outline first the basic model (Fig. 1) to be described in detail later (*Appendix*). The cell is characterized by the biological interplay between the genetic and the bioelectric networks and is connected to the neighboring cells by the gap junctions [16]. The results provide a qualitative interpretation of previous experimental data by means of two generic polarizing (*pol*) and depolarizing (*dep*) ion channel families (Fig. 1). The *dep* and *pol* channel conductances are modulated by the voltage-dependent transcriptional processes of the respective channel proteins. In this way, the polarized and depolarized cell states can be transcriptionally influenced by the membrane potential through the local concentrations of signaling molecules and ions [40] because these concentrations depend on the electric potential pattern. Other post-translational regulations, e.g. the external blocking of the channels, can also be introduced [16].

At the multicellular level, the cells are coupled together by gap junctions (Fig. 1). The junction conductance can be regulated not only by transcriptional processes [40] but also by the relative potentials of the neighboring cells [46]. As an illustrative case, Fig. 2a shows a central cell in contact with quiescent cells that are in a stable polarized state [16]. The potential of the central cell can be in an oscillatory regime when the intercellular coupling is zero ($G^0/G_{dep}^0 = 0$) or weak ($G^0/G_{dep}^0 = 0.01$) where G_{dep}^0 is the *dep* channel conductance. However, a strong enough coupling ($G^0/G_{dep}^0 = 0.02$) generates a *community effect* that hinders the potential oscillation of the central cell, which attains a bioelectrical state similar to quiescent polarized state to its neighboring cells, as shown in Fig. 2b [16]. Experimentally, the complex interplay between the bioelectrical network with the local genetic networks allows the spatio-temporal regionalization of cell potentials in stationary and oscillatory patterns that can codify instructive morphological information [8,16,28]. Note in particular that the oscillatory regime is one of the bioelectrical signs of the cell cycle [16,23].

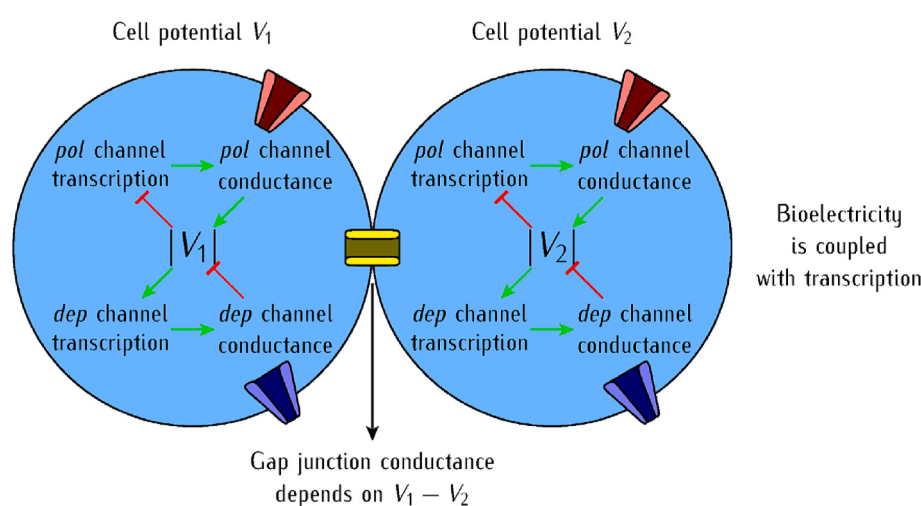


Fig. 1. Scheme of the coupling between bioelectricity and transcription for the *pol* and *dep* channels at the single-cell level. The counteracting actions of these channels aim at keeping the cell potential V_1 within a physiological window. The *pol* channel transcription is decreased (red segment) by $|V_1|$, which is the *absolute value* of V_1 . This *negative* regulation of the *pol* channel attempts to repolarize the cell at sufficiently low $|V_1|$. The *dep* channel transcription is increased (green arrow) by $|V_1|$. This *positive* regulation of the *dep* channel attempt to depolarize the cell at high $|V_1|$. Analogous processes affect cell 2. The multicellular network connectivity is provided by the intercellular gap junction, whose conductance is regulated by the cell potentials difference $V_1 - V_2$.

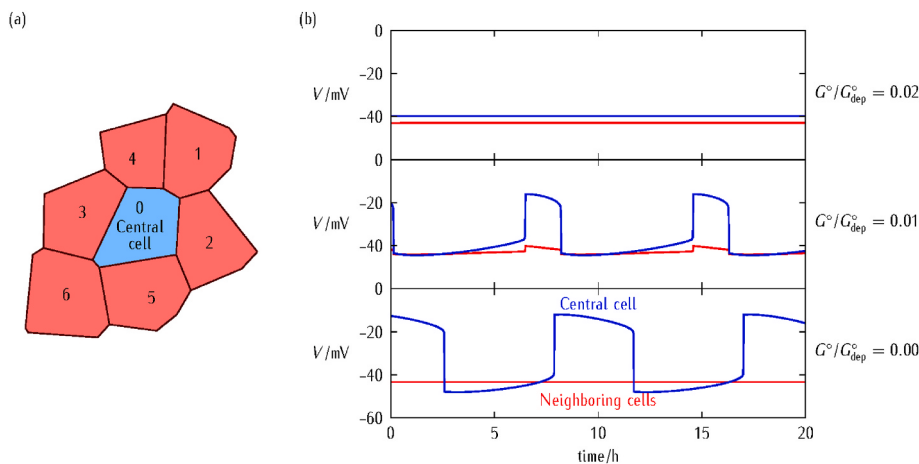


Fig. 2. (a) Six cells in a quiescent polarized state are coupled to a central cell through intercellular gap junctions whose conductances G_{ij} are regulated by the potential differences $V_i - V_0$ (Fig. 1 and Appendix). Each intercellular conductance can attain a maximum value G^* . (b) For a certain range of bioelectrical parameters, the potential of the central cell (blue curves) can oscillate when the intercellular coupling is zero ($G^*/G_{\text{dep}}^* = 0$) or weak ($G^*/G_{\text{dep}}^* = 0.01$). However, increasing the coupling ($G^*/G_{\text{dep}}^* = 0.02$) generates a community effect that hinders the oscillation of the central cell, which attains then a quiescent polarized state similar to those of its neighboring cells (red curves). Adapted with permission from Ref. [16].

3. Simulation results

3.1. Multicellular oscillations

The model biosystem of Fig. 3 consists of a two-dimensional array of $N = 1165$ cells with a *left-right* or an *anterior-posterior* morphology regulated by the *pol* channel protein transcription (Fig. 1). This minimal idealization leads to an *integration/segregation topology* of polarized and depolarized regions. The information of the location of a cell within the array can be bioelectrically encoded and compose an instructive transcriptional pattern for different gene-expression regions of the channel proteins. Fig. 3a shows the total current (I)–cell potential (V) curves and the cell potential bi-stability obtained from the two counteracting *pol* and *dep* voltage-gated channels of Fig. 1 [27,47,48]. Experimentally, the interplay between outward and inward currents can produce bi-stable potentials and neurophysiological oscillations [49], being also typical of pancreatic islets [50], Purkinje neurons in vitro [51], human cardiomyocytes [52], and biosynthetic tissues [38,53]. In general, polarized cell states are associated with cell differentiation and quiescence, and depolarized states are found in proliferating cells [8]. It is conceivable that a bioelectrical bi-stability can eventually be transduced into downstream biochemical processes where genes are in binary *on/off* states regulated by signaling ions and molecules. Memory implementation in proteins [54] can also show feedback mechanisms and bi-stability phenomena.

In the upper row of Fig. 3a, cells 1 correspond to the *left* region of the system and cells 2 to the *right* region. Usually, cells 2 are polarized (red color) while cells 1 are depolarized (blue color). However, they may temporarily change their polarization state. Note that the cells in the bulk of the respective *left* and *right* regions have similar *left* and *right* region curves. The curves are overlaid in the first plot because the whole system is in the polarized state.

The bi-stability of Fig. 3a results from the dynamical equation for dV/dt described in detail in the *Appendix* and allows the formation of regions with different cell potentials in the multicellular system. These regions have been predicted theoretically [27,28,55–57] and observed experimentally [38,53,58]. The interface between the regions can be stationary or mobile, depending on the values of the *pol* and *dep* conductances, which can be regulated by their respective bioelectrical and transcriptional states (Fig. 1). The cell potential to transcription coupling can make the system resilient to small perturbations at the single-cell and multicellular levels [16,40]. However, for a high enough

spatio-temporal inhomogeneity, depolarizing and polarizing waves can propagate through the system [38,39,50,53,58]. The visualization of the electric potential regionalization by voltage-sensitive indicators [59,60], including the intercellular junction coupling [61], suggests that bioelectrical patterns can be correlated with local gene-expression [8]. Morphologically instructive regions characterized by polarized and depolarized cell potentials have been described in development and tumorigenesis [8–10,62].

We focus now on the time-dependent potentials of Fig. 3b. All cells have a *dep* channel transcription rate $r_{m,\text{dep}}^0 = 1 \text{ min}^{-1}$. The cells in the *right* region have a *pol* rate $r_{m,\text{pol}}^0 = 1.5 \text{ min}^{-1} > r_{m,\text{dep}}^0$ and those in the *left* region have a lower *pol* transcription rate $r_{m,\text{pol}}^0 < r_{m,\text{dep}}^0$. This spatial inhomogeneity in $r_{m,\text{pol}}^0$ could result from different environmental conditions and developmental stages [8,16]. In Fig. 3a (first plot), all cells have similar current – cell potential curves because at $t = 0$ all cells are assumed to be in the polarized state characteristic of the *right* region. Therefore, the system regionalization that will result from the long-term transcriptional effects have not developed yet. These transcriptional effects are due to: (i) the rate constants $r_{m,\text{pol}}^0 < r_{m,\text{dep}}^0$ and $r_{m,\text{pol}}^0 > r_{m,\text{dep}}^0$ assumed in the *left* and *right* regions, respectively, and (ii) the different cell potential regulation of the transcription rate constants $r_{m,\text{pol}}(V)$ and $r_{m,\text{dep}}(V)$. Note that the transcription rate of the *dep* channel protein follows a *positive* cell potential regulation and that of the *pol* channel follows a *negative* cell potential regulation (Fig. 1). Thus, the polarized cell potential V increases the *dep* channel rate $r_{m,\text{dep}}(V)$ but decreases the *pol* channel rate $r_{m,\text{pol}}(V)$, creating a depolarized *left* region that coexists with the polarized *right* region in Fig. 3a (second plot). An interplay between cell potential and channel transcription has also been introduced in neuron models [63], illustrating another of many commonalities between neural and non-neural tissues.

Eventually, a depolarization wave develops and crosses the system from *left* to *right* because of the bi-stable potential of the cells in the *right* region (Fig. 3a) and the non-zero connectivity provided by the intercellular junctions. At longer times, the counteracting regulations of $r_{m,\text{dep}}(V)$ and $r_{m,\text{pol}}(V)$ with V , together with the rate constant $r_{m,\text{pol}}^0 > r_{m,\text{dep}}^0$ in the *right* region and the multicellular coupling, provokes a repolarization wave that crosses the system, this time from *right* to *left* in Fig. 3a (third plot). The oscillations are established when the depolarized state is eventually recovered in the *left* region (fourth plot) due to (i) the different rates $r_{m,\text{dep}}^0 > r_{m,\text{pol}}^0$ of this region and (ii) the *negative* cell

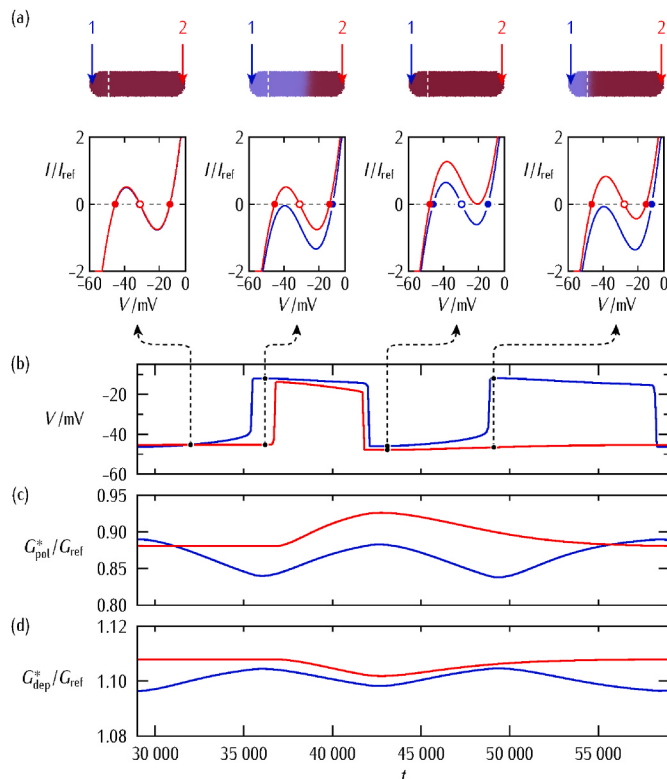


Fig. 3. (a) A multicellular system composed of $N = 1165$ cells with a boundary (white dashed line) separating the *left* and *right* regions (*top*). The rate constants that modulate the transcription of the *dep* and *pol* channel proteins are $r_{\text{m},\text{dep}}^0 = 1 \text{ min}^{-1}$ and $r_{\text{m},\text{pol}}^0$, respectively. The cells in the *left* region have $r_{\text{m},\text{pol}}^0 = 0.75 \text{ min}^{-1}$ while those in the *right* region have $r_{\text{m},\text{pol}}^0 = 1.5 \text{ min}^{-1}$. The total dimensionless current (I/I_{ref}) – cell potential (V) curves of cells 1 (*left* region of the system) and 2 (*right* region), where the reference current I_{ref} and the channel conductance G_{ref} are related as $I_{\text{ref}}/G_{\text{ref}} = 1 \text{ mV}$ (*bottom*). The potential V bi-stability results from the counteracting action of the *pol* and *dep* voltage-gated channels. The stable polarized (red circle) and depolarized (blue circle) cell membrane potentials correspond to the condition of zero total current. The current-potential curves in the four plots are different because the channel conductances G_{dep}^* and G_{pol}^* change with time. Note the multicellular potential patterns that result from the distinct single-cell polarized and depolarized states at different times. (b) The cell potentials V_1 and V_2 as a function of time t . (c) The *pol* channel conductances G_{pol}^* of cells 1 and 2 follow the behavior of the cell potentials because of the coupling between protein transcription and bioelectricity. (d) The *dep* channel conductances G_{dep}^* of cells 1 and 2. In the simulations, the junction conductance G^0 , normalized to a reference value G_{ref} , is $G^0/G_{\text{ref}} = 0.5$. For a cell capacitance $C = 100 \text{ pF}$ and a reference channel conductance $G_{\text{ref}} = 100 \text{ pS}$, the time unit is 1 s, so that $t = 60\,000$ corresponds to 17 h.

potential regulation of the *pol* channel.

The correspondence between the oscillatory cell potentials and the potential-dependent channel conductances (Fig. 3b, c, and 3d) arises from the coupling between electrical (cell potential) and transcriptional (channel mRNAs and proteins concentrations) magnitudes through the rate constants $r_{\text{m},\text{dep}}(V)$ and $r_{\text{m},\text{pol}}(V)$, see Appendix. Thus, the expression of the channel proteins regulates the cell potential and, in turn, the cell potential regulates the protein expression. This feedback results in oscillatory phenomena characterized by long-term transcriptional times, in the range 1–10 h (Fig. 3b), compared with the relatively fast electrical responses [40]. In the case of additional diffusion-reaction processes, experimental times could be much longer for systems with a high number of cells [56].

The complex multi-rhythmicity generated by the different couplings

observed in cellular rhythms and circadian clocks has been analyzed previously [64–66]. Also, long-range bioelectrical integration supported by gap junctions has been reported in oncogene-mediated tumorigenesis in *Xenopus laevis* embryos [67], long-distance control of brain morphogenesis in frog embryos [29,58], and during *Xenopus* hindlimb regenerative response [68]. Here, we have concentrated on the coupling between bioelectrical and transcriptional rhythms, paying attention to the long-range integration of the single-cell states to the multicellular level.

3.2. Effects of relative size, rate transcription, and intercellular conductance

Fig. 3b shows that cells 1 and 2 in the *left* and *right* regions can be coupled in phase and antiphase states, suggesting the possibility of a *spatio-temporal coding* based on the different bioelectrical and transcriptional states of distinct system regions. This coding can be further modulated by the relative size (Fig. 4) and transcription rate constant $r_{\text{m},\text{pol}}^0$ (Fig. 5) of the *left* region, as well as by the junction conductance that parametrizes the system connectivity (Fig. 6).

Fig. 4 shows that the duration of the depolarized periods of V_1 increases with the size of the *left* region because of the enhanced community effect until it approaches the time duration of the polarized value of V_2 , which marks the onset of synchronization. Fig. 5 shows the effect of the rate $r_{\text{m},\text{pol}}^0$ in the *left* region. For $r_{\text{m},\text{pol}}^0 = 0.65 \text{ min}^{-1}$, cells 1 and 2 are not coupled: the *left* region potential V_1 is depolarized because of the dominant rate $r_{\text{m},\text{dep}}^0 > r_{\text{m},\text{pol}}^0$, as shown by cell potential V_1 , while the

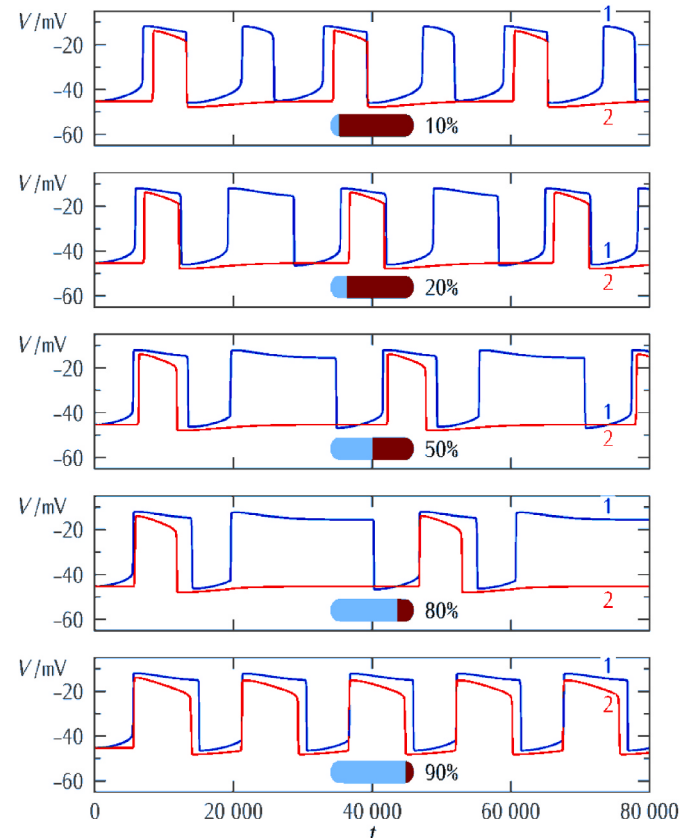


Fig. 4. Increasing the size of the *left* region from 10 % to 80 % of the multicellular system gives larger stability times for the depolarized values of V_1 (blue curves). Synchronization of potentials V_1 (*left* region) and V_2 (*right* region) is observed when the *left* region is 90 % of the multicellular system. In the simulations, the *left* region has a *pol* rate constant $r_{\text{m},\text{pol}}^0 = 0.75 \text{ min}^{-1}$ and the junction conductance is $G^0/G_{\text{ref}} = 0.5$.

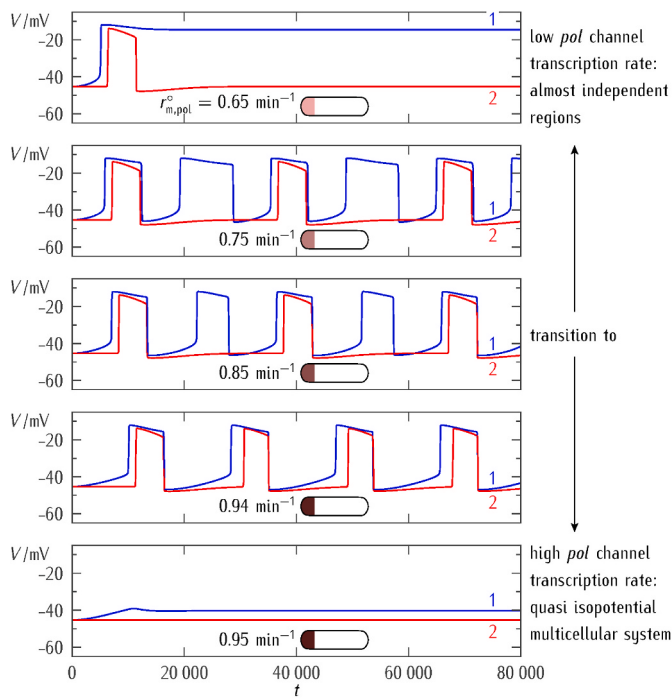


Fig. 5. Relatively small changes in the transcription rate can result in significantly different bioelectrical states and, at high enough transcription rates (bottom), synchronization of the long-distance cell potentials is observed. The cell potentials V_1 and V_2 vs. t for different *pol* channel transcriptional rates in the *left* region, from $r_{m,pol}^0 = 0.65 \text{ min}^{-1} < r_{m,dep}^0$ to $r_{m,pol}^0 = 0.95 \text{ min}^{-1} \approx r_{m,dep}^0$. For the lowest rate, the *left* and *right* regions are almost independent. Increasing $r_{m,pol}^0$ to $r_{m,dep}^0$ permits the coupling of these regions, giving phase and antiphase oscillations. An almost isopotential multicellular system, with polarized V_1 and V_2 , is observed for $r_{m,pol}^0 = 0.95 \text{ min}^{-1} \approx r_{m,dep}^0$. The *left* region size extends to 20 % of the total multicellular system and the junction conductance is $G^0/G_{ref} = 0.5$.

right region potential V_2 repolarizes after a transient depolarization period. However, oscillatory coupling, including the synchronization of these cell potentials, is observed for higher values of $r_{m,pol}^0$. For $r_{m,pol}^0 = 0.95 \text{ min}^{-1} \approx r_{m,dep}^0 = 1.0 \text{ min}^{-1}$, the potentials reach steady-state polarized values, giving a quasi-isopotential multicellular system. Experimentally, changes in the protein synthesis rate could be implemented by the microinjection of the mRNA that encodes the channel protein [8,58,59]. In addition to these slow transcriptional processes, individual conductances can also be modulated by a variety of inputs, including chemical ligands, light, heat, and mechanical effects [8,13,19,60].

Fig. 6 shows the effect of the intercellular gap junction conductance G^0/G_{ref} (Fig. 2). Very low values of G^0/G_{ref} make the cells to behave independently, so that the *left* region becomes depolarized because $r_{m,pol}^0 < r_{m,dep}^0$ in this region while the bi-stable *right* region remains polarized. On the contrary, very high values of G^0/G_{ref} lead again to an isopotential system dominated by the *pol* region (*right*) that is larger than the *dep* region (*left*). As in Figs. 4 and 5, synchronization of the cell potentials V_1 and V_2 , is also possible for intermediate values of G^0/G_{ref} because of the interaction between neighboring cells. Then, decreasing the intercellular connectivity from the synchronization regime immediately causes a phase shift in these cell potentials and a strong decrease can inhibit the wave propagation. The external blocking of the junction conductance can be realized by specific ions and molecules, producing changes in the instructive patterns that eventually result in significant morphological alterations [69,70].

The sharpness of the cell potential boundary depends on both the

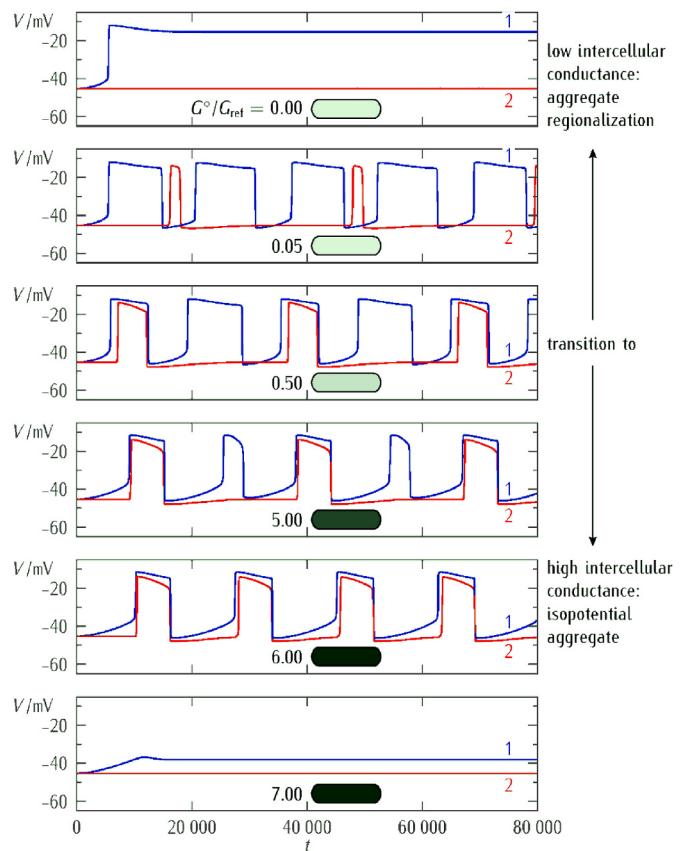


Fig. 6. Transitions between different bioelectrical states can be observed by regulating the conductance G^0/G_{ref} of the intercellular gap junctions. At zero coupling (top), the *left* and *right* regions are independent and show depolarized and polarized regions, respectively. On the contrary, at high intercellular connectivity, an almost isopotential multicellular system characterized by intermediate values of V_1 (*left* region, blue) and V_2 (*right* region, red) is obtained (bottom). Intermediate values of G^0/G_{ref} allow the coupling of the *left* and *right* regions in phase and antiphase oscillations, thus leading to the synchronization of distant cell potentials. The *left* region size extends to 20 % of the total multicellular system and has a *pol* transcription rate constant $r_{m,pol}^0 = 0.75 \text{ min}^{-1}$.

relative polarization states of the neighboring cells and the maximum junction conductance (Fig. 2). In general, the cell polarization state in the bi-stability region of the current-voltage curves of Fig. 3a is determined by the relative values of the *dep* and *pol* conductances. However, the gap junction conductance is not a single-cell but an intercellular property: it achieves a maximum within a polarized or depolarized patch and a minimum at the interface between polarized and depolarized patches, where the cells are largely decoupled (Appendix). This characteristic contributes significantly to the displacement of the interfacial region following polarization and depolarization waves.

The spatial patterning of differentiation during early neural commitment has been associated with a highly dynamic intercellular transport [71] and the gap junction plasticity is known to regulate network-wide oscillations, phase synchronization, and large-scale integration patterns [16,72,73]. The different phase locking synchrony of potentials V_1 and V_2 , obtained for intermediate values of G^0/G_{ref} in Fig. 6, suggests that a dynamic connectivity could allow large-scale integration over distinct frequencies. In this way, multicellular aggregates of non-excitable cells could establish transient bioelectrical regionalizations to develop locally different transcriptional programs, as it has been observed for distinct bioelectric pre-patterns in face and brain development (reviewed in Ref. [8]).

3.3. Bioelectric and transcriptional spatio-temporal bands

Interestingly, four *dep – pol – dep – pol* transient regions with mobile interfacial regions can be observed in the multicellular aggregate (Fig. 7) when the intercellular connectivity is low. In this case, *pol* and *dep* waves can move across the system (see video *Mobile Interfacial Regions* in the *Supplementary Material*). The resulting non-stationary bands appear when the intercellular junction conductance, and thus the propagation velocity, are so low that the transcriptional processes provoke the emergence of a new *pol* region (time $t = 44100$) before than the *dep* wave has had time to reach the *right* region. These results demonstrate the rich biophysical dynamics of the model simulations.

As a possible limitation of the above results, we note that the establishment of large-scale bioelectric circuits should depend on the tissue dimensionality. We have analyzed two-dimensional (2D) model tissues and 1D linear chains of multicellular aggregates [16]. However, it could be expected that extending the simulations into the 3D space should give even more significant community effects because of the increase in the number of neighboring cells that can influence the bioelectrical state of a central cell.

Experimentally, symmetry breaking into regions with different biochemical [30–32] and bioelectrical domains [8,38,53,74,75] has

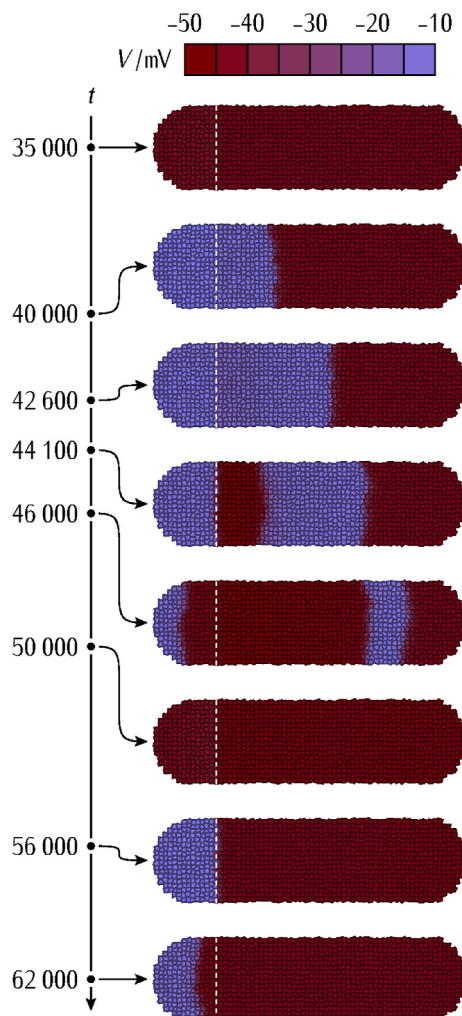


Fig. 7. A depolarization wave can propagate across the multicellular system for the relatively low junction conductance $G^0/G_{\text{ref}} = 0.05$, as evidenced by the spatio-temporal bands of alternate *dep* and *pol* regions. The cells in the *left* region size extend to 20 % of the total system and have a *pol* transcription rate constant $r_{m,\text{pol}}^0 = 0.75 \text{ min}^{-1}$. See also the video *Mobile Interface Regions*.

been described in development, wounding, and artificial tissues. In particular, bi-stability, interfacial phenomena, wave propagation, and community effects are characteristic of patterns of cell potentials [38,39, 55–57]. Oscillatory bioelectrical phenomena have also been observed in bacterial [24,25] and cell [76–78] communities, including quasi-periodic signals in the low frequency range. Experimentally, the results of Fig. 3–7 can be of qualitative interest to these systems because of the central role of oscillatory cell membrane potentials.

4. Model validation and limitations

A crucial question is *how bioelectrical networks could contribute to the spatio-temporal integration needed for morphogenetic robustness during embryogenesis and regeneration*, where coordination between distant regions mediates the information transfer. We aim here at emphasizing *new biophysical insights* which can lead to future experiments, looking for phenomena that might not have been noted previously. In particular, we explore the connections between spatial heterogeneity and multicellular oscillations that are in phase, out of phase, or coupled at different harmonic frequencies. While spatially extended systems of coupled biological oscillators have been studied extensively by others, our study explores a new physical model with the different timescales of bioelectrical and transcriptional-translational phenomena. Our experimental basis is the fact is that polarized and depolarized potential regions are clearly visible in tissues and model animals. In particular, differentiated and quiescent cells are usually polarized with respect to embryonic and tumor cells, which tend to be depolarized [8]. Also, oscillatory electrical potentials are observed in different spatio-temporal scales of biological organization [16].

Note that, from an operational viewpoint, it should be feasible to control electric potentials and currents at a limited number of physical locations [40]. In particular, bioelectric networks can be manipulated by changes in the regulation of target channel proteins (the case of the *pol* channel transcription rate $r_{m,\text{pol}}^0$ here), the microenvironmental ionic concentrations [16], and the blocking of specific channels [13,40,56] and intercellular junctions (the case of the conductance G^0 here) [16, 69]. Also, charged nanoparticles can be used in external actions on cell potentials, as observed by flux cytometry, dyes, and fluorescence microscopy techniques. Indeed, the simulations suggest that the spatial distribution of charged nanoparticles should follow the multicellular pattern of cell potentials. For instance, accumulation of positively-charged nanoparticles should be enhanced around polarized (more negative) cells compared to depolarized cells [16].

Experimentally, bioelectrical patterns of cell potentials showing a depolarized region in wild-type planaria are instructive for the worm anatomy. The use of RNAi or channel drugs can modulate the cell polarization patterns, alter the downstream expression of axial polarity genes, and produce two-headed or no-headed worms [8,16]. The results clearly suggest the correlation between the multicellular electrical patterns and the spatio-temporal distribution of signalling ions and molecules that modulate large-scale expression patterns. This biophysical-biochemical feedback is central to regeneration and dynamic maintenance of correct morphology [8,16]. As a possible limitation, note here that our model is bioelectrically-focused and ignores additional effects due to ligand-gated and biomechanical ion channels. However, while a wide variety of channels can exist in the membrane, voltage-gated channels are crucial to cell bioelectricity because they may influence the counteracting dynamics typical of many physiological functions. Starting from this qualitative experimental fact, the model assumes the coarse-graining of all relevant channel conductances into two generic *pol* and *dep* channels that promote the polarized and depolarized cell states, respectively. Although we do not claim any generality here, counteracting actions between a reduced number of channels are experimentally relevant:

- i. Homeostatic ion channel regulation, which is central to neurons, can be influenced by generic voltage-gated ion channel populations whose mRNA levels are regulated via transcription regulatory pathways where the transcriptional coupling between calcium levels and the cell membrane potential is essential [49];
- ii. The interplay between *dep* and *pol* (sodium, calcium, and potassium) channels are involved in crucial steps of the cell cycle [23];
- iii. The opposite activity of voltage-gated depolarizing and polarizing channels may influence circadian clocks [22];
- iv. The concerted activity of counteracting voltage-gated channels is central to pacemaking regulation [16,52];
- v. The combined action of the Kir and HCN2 channels plays a significant role in the endogenous voltage pre-patterns of brain development [58];
- vi. A small number of key voltage-gated channels can control bioelectrical phenomena in engineered tissues [53]; and
- vii. A dynamic balance between a small number of voltage-gated channels can be established by only a calcium channel (Cav1.2) coupled to an inwardly rectifying potassium channel (K_i2.1), resulting in a voltage-gated circuit that participates in the control of gene expression [20]. Certainly, many biochemical pathways are essential to induce expression of differentiation factors but channel bioelectricity influence also the downregulation timing of pluripotency genes [21]. Thus, we believe that the extension of these single-cell characteristics to a tissue may lead to instructive bioelectrical patterns at the multicellular level [8,16].

Regarding the network topology, a possible model limitation is the fixed geometry (Fig. S2). Note however that the strength of the intercellular connectivity depends on both the maximum junction conductance G^o (Fig. 6) and the difference between the neighboring cell potentials so that it can effectively change with the polarization states of these cells (Fig. 2). Thus, the intercellular connectivity is not a *static* but a *dynamic* characteristic, defined at the high-level configuration of the multicellular aggregate, that modulates the propagation of bioelectrical signals (Figs. 6 and 7, and S3). Because of the coupling between bioelectricity and transcription [8,16], interrogating and modifying the connectivity by using probe ions and molecules should offer additional opportunities for the external control of the multicellular aggregate [40]. In addition, well-defined biosynthetic excitable tissues [38,51] may also be used to establish the roles of specific ion channels and gap junctions and their mutations. While extrapolations to tissue-level electrophysiology are not always evident, biosynthetic multicellular aggregates should permit controlled experiments to check model simulations and, in particular, the propagation of bioelectrical waves [38,51].

Additional experimental relevances of the simulations are brain teratogenesis and bioelectrically-induced long-range repair, where multicellular electric potential patterns behave as a bioelectrical memory for gene expression, brain morphology, and learning [58]. In particular, embryonic exposure to nicotine degrades this memory pattern and leads to aberrant gene expression, brain morphology defects, and impaired learning. Transplanting a new bioelectrical module, the HCN2 channel tissue, onto nicotine-exposed embryos contributes to the restoration of the correct memory pattern, as shown by voltage reporter dyes and gene expression [58]. Here, previous model simulations qualitatively predict a distant channel-mediated rescue of the bioelectrical memory pattern in nicotine-exposed embryos under different conditions concerning the size and position of the inserted channel tissue [58].

Concerning biological oscillations, note that while they play critical roles, their function is not always clear [79–82]. We have studied here the case of bioelectrical and biochemical oscillations that are coupled at both the individual cell and the multicellular levels. In particular, the simulation results obtained in Fig. 3–6 and S3 suggest an information transmission code based on the absolute level, time duration, and

frequency of single-cell potentials [83]. At the multicellular level, different regionalizations can be encoded by *long-distance* cell potentials that oscillate in the *dep* (*D*)-phase, *pol* (*P*)-phase, and *dep/pol* (*D/P*)-antiphase. Some approximate code sequences are $P - D - P - (D/P) - P - D - P - (D/P) - \dots$ in Fig. 3 (20 %), $P - D - P - D - \dots$ in Fig. 3 (90 %), and $P - (D/P) - (P/D) - (D/P) - P - (D/P) - (P/D) - (D/P) - \dots$ in Fig. 6 ($G^o/G_{ref} = 0.05$); see also Fig. S3 for the multicellular time snapshots. Note here that these cell potential sequences can correspond to the level and time sequences of signaling ions and molecules whose local activity in different multicellular physiological states is closely related to bioelectrical signals [8,40]. In a loose analogy, the fast-wave patterns of neural networks can reflect different mental states [35, 84–86]. Remarkably, large-scale integration and synchronization are also characteristic of these networks [73].

The oscillatory phenomena of Fig. 4–7 originate from the *symmetry breaking* assumed in Fig. 3, where the cells in the *left region* have a *pol* channel transcription rate constant different than those in the *right region*. This initial condition may allow a mass of undifferentiated cells to initiate a spatio-temporal regionalization that defines morphologically-instructive patterns because different bioelectrical states correspond to distinct transcriptional states across the multicellular aggregate. While a multitude of intracellular signal transducers and biochemical pathways modulate differentiation, channel bioelectricity controls also the downregulation timing of pluripotency genes; for instance, membrane potential drives the exit from pluripotency and cell fate commitment via calcium entry in the onset of embryonic differentiation, see Fig. 7b of Ref. [21]. In this case, potassium channels set the polarized cell potential, which keeps voltage-gated calcium channels inactivated and avoids the high calcium levels required for the downstream processes leading to pluripotency.

Interestingly, cells need to estimate their location within a multicellular aggregate for local differentiation processes. The bioelectrical gradients that couple cell potentials to transcription rates provide a rough idea of where a single-cell is in the multicellular ensemble, thus controlling local differentiation processes that can switch *on* and *off* crucial parts of the genome. Because cells constantly monitor their environmental signals, including those from the neighboring cell states, the single-cell state at a given location of the multicellular aggregate provides the dynamic information characteristic of the developmental stages. Note also that the results of Fig. 3–7 show that boundary cells can use moving bioelectrical interfaces to establish instructive spatio-temporal modules. At the multicellular aggregate level, these time-dependent modules suggest that development can involve not only cell migration but also local changes in the spatially-fixed cell states that are induced by polarization and depolarization waves, as shown by the simulations.

At this point, it is tempting to speculate that the *polarized/depolarized* bi-stability characteristic of the above coding signals can be transduced into the corresponding binary *on/off* gene states because of the interplay between bioelectricity and transcription [19–21]. In this way, *cell bioelectricity could contribute to the integration of transcriptional states in a multicellular aggregate*. If different, spatially-separated regions of the multicellular system are bioelectrically coupled, external interventions on the cells in one region of the system should influence outcomes in other regions. This model prediction can be relevant to experiments showing long-range communication in injured froglets [68] and the correction of defective electric potential patterns that is induced by manipulating bioelectric states of distant cells in multicellular systems [40,58,87].

In summary, we believe that bioelectrical models can provide useful qualitative insights into the interplay between transcription and bioelectricity. New opportunities emerge at the *intermediate scale* of endogenous multicellular fields, which constitutes a complementary approach to the *small scale* of molecular mechanisms and the *large scale* characteristic of applying electrical fields to tissues and organs. Certainly, the model simplicity cannot give a quantitative description of

the biological complexity and diversity found in real cases but a tentative experimental procedure would be to find out that intermediate step whose transduction is rate limiting and then devise specific actions on it. Note however that these actions should be system-dependent in the sense that a previous knowledge of the particular channels and bio-physical mechanisms to be addressed is needed for the correcting actions to be implemented [40,58,87].

5. Conclusions

In neural networks of excitable cells, significant electrical activity is observed in early neuronal development [88]. Also, bioelectrical potentials are involved in the excitation–transcription coupling that underlies long-term potentiation and memory because membrane depolarization at the synapse and in the soma drives Ca^{2+} entry via voltage-gated channels, thus activating downstream transcriptional signalling cascades [89]. Long-term plasticity in mean-field neuronal population models has also been studied in terms of calcium-dependent plasticity models [90]. In different experimental contexts, the electrophysiological role of ion channels has been emphasized in previous models of biological tissues [91] and pancreatic β -cell hubs [92].

In our computational biology study, we have explored how the coupling between bioelectricity and transcription can influence the long-distance coordination that mediates the information transfer during embryogenesis and regeneration in networks of non-excitable cells. This spatio-temporal coordination requires a morphogenetic robustness that can be provided by bioelectrical networks. Our simulations on the coupling between bioelectrical and transcriptional signals at the single-cell and multicellular levels suggest that spatial regionalizations can be encoded by distant cell potentials that oscillate in depolarized and polarized states. The oscillations enable a spatio-temporal coding for different regions of the multicellular aggregate based on their distinct polarization states. The electric potential patterns characteristic of different developmental and regeneration processes and stages are correlated with the spatial distributions of ions, neurotransmitters, and

transcription activators. Hence, due to the different hierarchy of characteristic experimental times, bioelectricity can act as a tractable template to much slower biochemical signals [8,16,85,93,94]. In this context, the non-specific character of electric potential may open new options for intervention in bioengineering and biomedical contexts, based on the pharmacological manipulation of the ion channels and gap junctions that modulate the instructive patterns toward desired tissue-level endpoints.

CRediT authorship contribution statement

Javier Cervera: Writing – review & editing, Software, Methodology, Investigation, Funding acquisition, Formal analysis, Conceptualization. **José A. Manzanares:** Writing – review & editing, Formal analysis, Conceptualization. **Michael Levin:** Writing – review & editing, Funding acquisition, Formal analysis, Conceptualization. **Salvador Mafe:** Writing – original draft, Methodology, Investigation, Formal analysis, Conceptualization.

Declaration of competing interest

M.L. is cofounder of the company Morphochemicals Inc., which operates in the regenerative medicine and hopes to do regeneration by bioelectric technology.

Acknowledgments

J.C., J.A.M., and S.M. acknowledge the support from the *Ministerio de Ciencia e Innovación* (Spain) and the European Regional Development Funds (FEDER), project PID2022-139953NB-I00. M.L. acknowledges the support by the Templeton World Charity Foundation (TWCF0606) and the Guy Foundation Family Trust (103733-00001). The study sponsors had no involvement in the study design, collection, analysis and interpretation of data, writing of the manuscript, and decision to submit the manuscript for publication.

Appendix A. Supplementary data

Supplementary data to this article can be found online at <https://doi.org/10.1016/j.combiomed.2024.108964>.

APPENDIX. VI. SIMULATION EQUATIONS AND PARAMETERS

A. Multicellular system

The model is based on two well-established experimental facts [8,16,40]: (i) the coexistence of adjacent depolarized and polarized neighboring regions in developmental, regeneration, and tumor processes and (ii) the possibility of describing the multicellular pattern dynamics in terms of average electric potentials. The coupling between bioelectrical and transcriptional networks concerns not only the local expression of ion channel and intercellular junction proteins but also the long-distance propagation of electrical signals. Thus, theoretical description is based on the cell potential V , which is defined as the negative electrical potential difference established between the cell inside and the external microenvironment (Fig. 8, top). The depolarized (*dep*) and polarized (*pol*) single-cell states correspond to low and high absolute values of V , respectively.

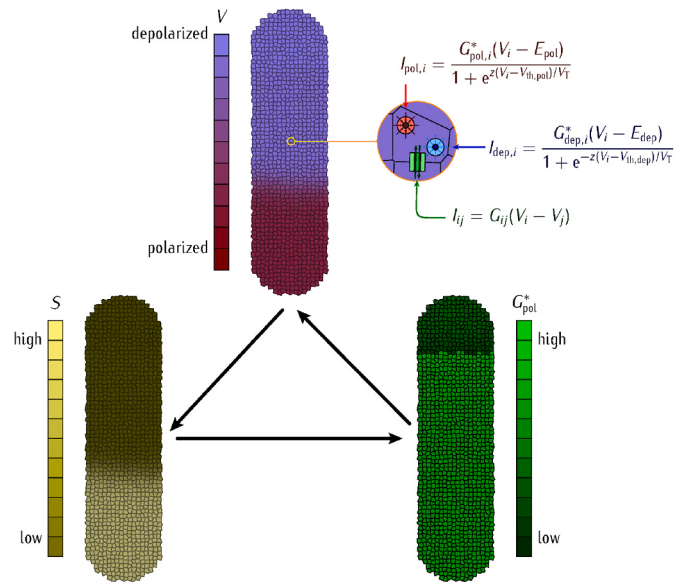


Fig. 8. The state of cell i ($i = 1, 2, \dots, N = 1165$) is characterized by the potential V_i that changes with time t because of the individual currents $I_{dep,i}$ and $I_{pol,i}$ through the voltage-gated channels with conductances $G_{dep,i} = G_{dep,i}^*/\{1 + \exp[-z(V_i - V_{th,dep})/V_T]\}$ and $G_{pol,i} = G_{pol,i}^*/\{1 + \exp[z(V_i - V_{th,pol})/V_T]\}$ of saturation values $G_{dep,i}^*$ and $G_{pol,i}^*$, and the intercellular currents $I_{ij} = G_{ij}(V_i - V_j)$ that flow through the junction conductance G_{ij} between neighboring cells i and j [16,40] (top), where $V_i - V_j$ is the intercellular potential difference. The spatial map of *dep* channel conductances is also shown (bottom, right). Typical system parameters are $G_k^* \approx 100$ pS, $E_{dep} = 0$ mV, $E_{pol} = -60$ mV, $V_{th,pol} = V_{th,dep} = -V_T = -26$ mV, and $z = 2$ [16]. The feedback between the local concentration S of a signaling ion or molecule influencing transcription that can be modulated by the cell potential via specific voltage-gated channels (bottom, left). In this model, the ion channels and the intercellular gap junctions allow the cells to iterate with time their individual states following the local changes in currents and potentials. Multicellular patterns emerge because of the position of a particular cell with respect to the neighboring cells and the external microenvironment.

The ionic conduction transporters in the cell membrane are simulated by generic *dep* and *pol* families of voltage-gated channels, with conductances G_{dep} and G_{pol} , that tend to establish the characteristic potentials E_{dep} and E_{pol} of the depolarized and polarized single-cell states [16]. These equilibrium potentials couple the cells with their microenvironment because they are determined by the external and internal ionic concentrations, which are established by additional membrane ion pumps and transporters [13]. Note that opening the voltage-gated channels causes an ionic current that may rapidly change the cell potential without significantly altering the ionic concentrations in short times. The experimental values for the reference currents (I_{ref}) and channel conductances (G_{ref}) give a typical order of magnitude potential $I_{ref}/G_{ref} = 1$ mV.

Fig. 8 shows two phenomenological equations for the current-voltage curves of the *dep* and *pol* channels that qualitatively describe the observed behavior in typical voltage-gated channels [16]. These equations are characterized by the channel gating charge number z , the threshold potentials $V_{th,pol}$ and $V_{th,dep}$, and the thermal potential $V_T = RT/F$, where R is the gas constant, T is the temperature, and F is the Faraday constant. While the potential difference across the cell membrane is primarily determined by the concentration ratio of the most permeable ion, the above voltage-gated conductances eventually result in potential-dependent permeabilities. For example, a normally polarized cell potential around -70 mV due to the intracellular (high) and extracellular (low) concentration of K^+ can be depolarized here to less negative values if the model voltage-gated conductance G_{pol} decreases, e.g. by introducing a potassium channel blocker, or by externally inducing a decreased expression of the corresponding channel protein, because these actions decrease the effective permeability to K^+ [13,16]. In this way, the individual cell states are regulated by the *dynamic balance* between the two voltage-gated currents together with the intercellular junction currents that modulates the *system connectivity* [16,40].

B. Coupling between cell bioelectricity and transcription

The coupling between bioelectricity and transcription results from the local correlation between cell potentials and signaling ions and molecules. Here, it is important to understand the role of the local concentration S . For instance, the calcium concentration, which is regulated by the conductances of many calcium channels, influences transcription, proliferation, wound healing, and synchronized oscillations. Also, local cell potentials can influence the distribution of nanoprobes such as charged nanoparticles because of the membrane charges and the resulting surface electric potential [16].

The local concentration S can be modulated by the cell potential via a specific voltage-gated transporter (Fig. 9, bottom), as in the opening of the calcium channels that follows cell depolarization [16]. On this experimental basis, we introduce now the transcription of the *dep* and *pol* channel proteins in terms of the mRNA (m_{dep} and m_{pol}) and protein (p_{dep} and p_{pol}) concentrations (Fig. 9a). The rate constants $r_{m,k}$ and $r_{p,k}$ ($k = pol, dep$) regulate the mRNA transcription and protein translation processes, which occur with the respective degradations rates $d_{m,k}$ and $d_{p,k}$. Note that, in this extended model incorporating transcription, the voltage-gated conductance G_k depends not only on the cell potential V (Fig. 8) but also on the protein concentration p_k (Fig. 9a). Because of this additional dependence, the conductance $G_k^*(p_k) = G_k^0 p_k / (p_{0,k} + p_k)$ assumes a Hill kinetics, where G_k^0 is the maximum conductance value. The constant concentration $p_{0,k}$ corresponds to half-maximum conductance $G_k^*(p_k = p_{0,k}) = G_k^0/2$. The above kinetic saturation of the *dep* and *pol* channel conductances arises from the finite values of the transcription and translation rates and may incorporate the limits imposed by the protein trafficking to and insertion in the cell membrane. The action of specific blockers can also be introduced by decreasing the effective values of the maximum conductance G_k^0 [13,16].

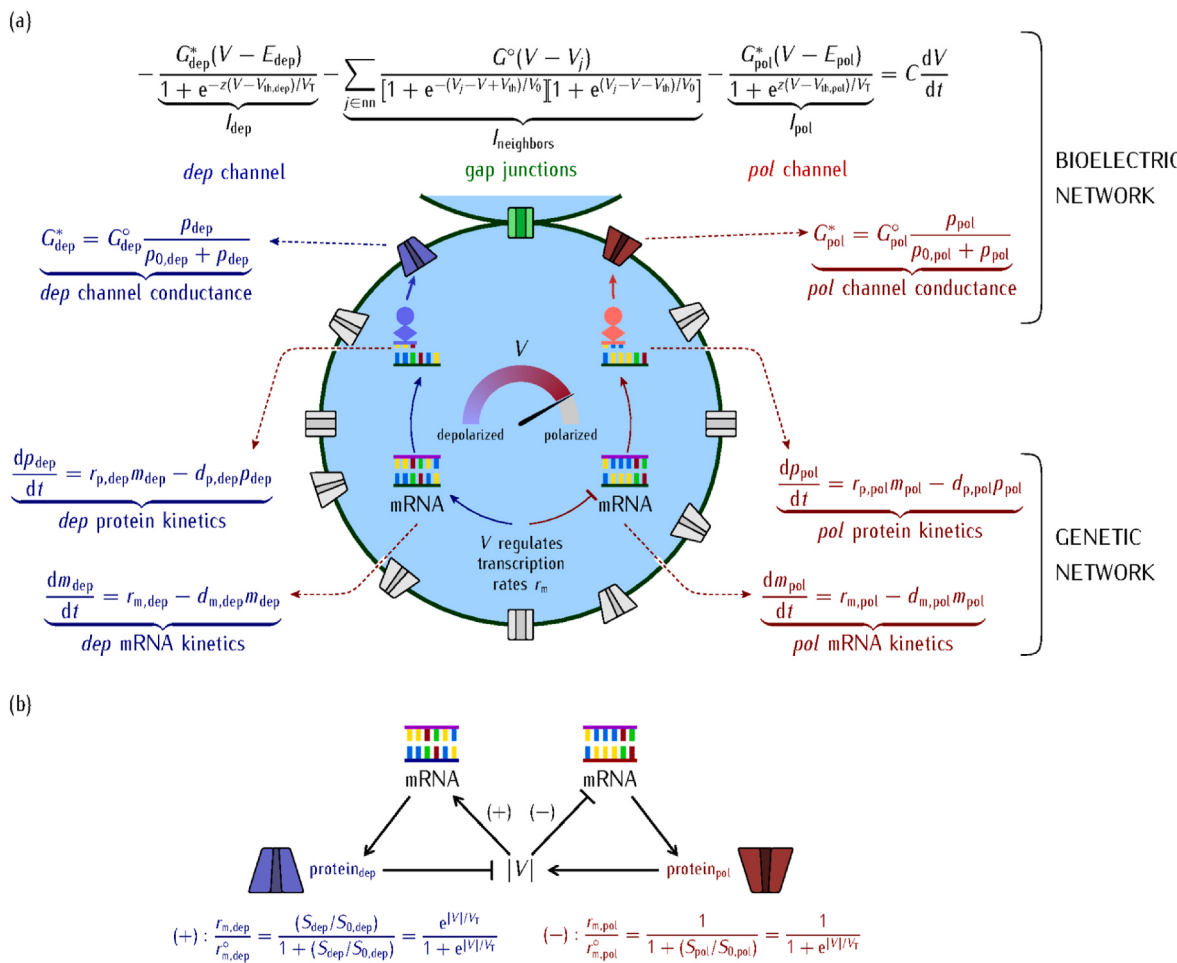


Fig. 9. (a) The coupling between bioelectricity and transcription regulates the *dep* and *pol* cell states through the respective channel proteins. The sum of currents through the intercellular gap junctions runs over nearest neighbors (nn) cells j . The single-cell sensitivity to electrical signals is characterized by the cell capacitance, which is in the range $C = 10 - 100 \text{ pF}$. (b) The resulting feedback leads to both transcriptional and post-translational dependences of the channel conductances on the cell potential V because of the voltage-dependent concentration S_k ($k = \text{pol}, \text{dep}$) of a signaling molecule or ion. Here, $S_{0,k}$ is a reference concentration. In this way, V couples the transcription of the two channels through the values of S_k , which leads to effective transcription rates that may show a positive (+) or negative (-) Hill kinetics regulation with V [16]. The particular scheme describing the feedback as well as the signaling ions or molecules should depend on the experimental biosystem. Typical values for all system parameters have been justified elsewhere [16,40] and are given below.

The coupling between transcription and bioelectricity of Fig. 9 gives cell potential-dependent mRNA transcription rates, $r_{m,k}(V)$, where $r_{m,k}(0) = r_{m,k}^0/2$, ($k = \text{pol}, \text{dep}$), are reference values. Thus, the cell potential V modulates the protein concentrations p_k and the resulting channel conductances G_k through the *transcription* (Fig. 9) while the channel conductances G_k modulate V through the *post-translational bioelectricity* (Fig. 8). This transcriptional and post-translational control of the channel protein expression can be tuned to each model biosystem. In particular, the feedback between bioelectricity and the genetic regulation networks should be *system specific*. Thus, other theoretical schemes different from that of Fig. 9 should be introduced in distinct experimental cases.

C. Intercellular voltage-gated gap junctions

Gap junctions are channels with dynamic conductances that confer intercellular plasticity, thus providing spatio-temporal correlations between bioelectricity and transcription at the multicellular level. Although the junction proteins may also have other biochemical and biomechanical functions, we focus on the electrical network effects, taking into account again a series of experimental facts (Fig. 10):

- the junction conductance can depend on the relative potential $V_i - V_j$ between cells (Fig. 10a) and attains a maximum value when neighboring cells have similar potentials [16]. Non-linear electrical behaviors can also be observed in the junctional current rectification at an electrical synapse [46]. In addition, the intercellular conductance depends on the particular junction protein. For instance, distinct connexin proteins such as Cx43 and Cx45 can show different voltage-gated behaviors and maximum conductances (Fig. 10b) [16,40];
- in general, both homotypic and heterotypic (e.g. Cx43/Cx45) junctions can be defined (Fig. 10b) [2]. Also, for a given connexin, the maximum effective conductance can depend on the protein expression level, which may change with the cell polarization state (Fig. 10b) [16]; and
- the biosystem can be regionalized into different multicellular modules showing distinct intercellular couplings because of the particular junction conductance values prevailing in each module (Fig. 10b). This spatial regionalization can be due to different junction expression over distinct modules. It could also be induced by junction blocking [13,16], using specific molecules in each multicellular module.

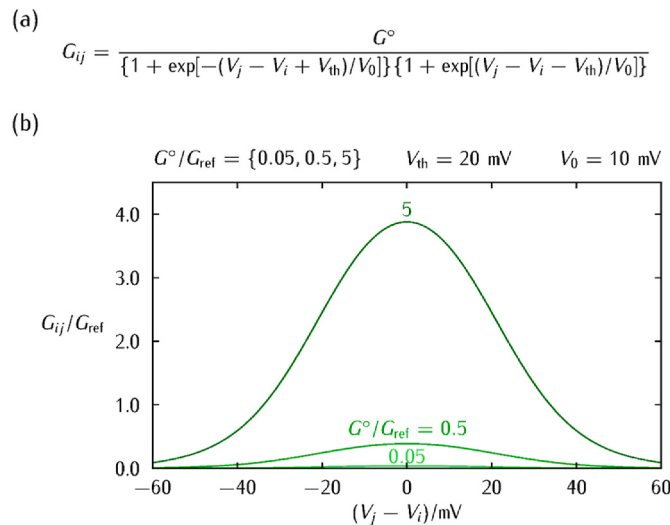


Fig. 10. (a) The junction conductances of two different connexin proteins characterized by the model equation and parameters [40]. (b) Experimentally, the effective junction conductance G_{ij} depends on the potential difference $V_i - V_j$ between neighboring cells. The voltage sensitivity characteristic of the junction protein can be incorporated through the reference potential V_0 . (b) In the simulations, we assume that all cells have maximum junction conductance G^o . The cases of strong, intermediate, and weak values of the maximum junction conductance G^o are shown. The junction parameters used in the simulations are given below.

D. Simulation parameters

We have established previously the typical ranges for the system parameters used [16]. Except for the rate constant $r_{m,pol}^o$ that regulates the mRNA transcription of the *pol* channel protein in the *left* region of the model network, all cells have the same parameters (Figs. 8 and 9) unless otherwise indicated. The cell capacitance is $C = 100 \text{ pF}$ and the equilibrium potentials are $E_{dep} = 0 \text{ mV}$ and $E_{pol} = -60 \text{ mV}$ [13,16]. For the channel conductances, we introduce the parameters $V_{th,dep} = V_{th,pol} = -V_T = -RT/F = -26 \text{ mV}$ and $z = 2$, together with the conductances $G_k^*(p_k) = G^o p_k / (p_{0,k} + p_k)$ ($k = dep, pol$), with $p_{0,dep} = p_{0,pol} = 80$, $G_{dep}^o/G_{ref} = 1.15$ and $G_{pol}^o/G_{ref} = 1$, where G_{ref} is a reference conductance, which is typically in the range of 0.1 nS [16].

For the cell potential-dependent mRNA kinetics, we introduce the rate constants $r_{m,dep} = r_{m,dep}^o e^{|V|/V_T} / (1 + e^{|V|/V_T})$ and $r_{m,pol} = r_{m,pol}^o / (1 + e^{|V|/V_T})$ where the order of magnitude of the rates are $r_{m,dep}^o = 1 \text{ min}^{-1}$, and $d_{m,dep} = d_{m,pol} = 0.02 \text{ min}^{-1}$ [16]. The cells in the *right* region have $r_{m,pol}^o = 1.5 \text{ min}^{-1} > r_{m,dep}^o$ and those in the *left* region have a lower rate constant in the range $r_{m,pol}^o = 0.65 - 0.95 \text{ min}^{-1} < r_{m,dep}^o$. The spatial inhomogeneity of $r_{m,pol}^o$ can be due to an endogenous process in a developing biosystem or an externally-induced local action [40]. As to the protein kinetics, we use the rate constants $r_{p,dep} = r_{p,pol} = 1 \text{ min}^{-1}$ and $d_{p,dep} = d_{p,pol} = 0.02 \text{ min}^{-1}$ [16].

For the intercellular gap junction, a spatially homogeneous distribution of maximum intercellular conductances G^o is assumed. The range of values introduced in the simulations is $G^o/G_{ref} = 0 - 7$, with the reference potentials $V_0 = 10 \text{ mV}$ and $V_{th} = 20 \text{ mV}$ [16,40].

References

- [1] M. Kerszberg, L. Wolpert, Specifying positional information in the embryo: looking beyond morphogens, *Cell* 130 (2007) 205.
- [2] H. Meinhardt, A. Gierer, Pattern formation by local self-activation and lateral inhibition, *Bioessays* 22 (2000) 753.
- [3] P. Müller, E. El-Sherif, A systems-level view of pattern formation mechanisms in development, *Dev. Biol.* 460 (2020) 1.
- [4] A.M. Tayar, E. Karzbrun, V. Noireaux, R.H. Bar-Ziv, Propagating gene expression fronts in a one-dimensional coupled system of artificial cells, *Nat. Phys.* 11 (2015) 1037.
- [5] M. Smart, A. Zilman, Emergent properties of collective gene-expression patterns in multicellular systems, *Cell Rep. Phys. Sci.* 4 (2023) 101247.
- [6] A. Mukherjee, Y. Huang, J. Elgeti, et al., Membrane potential as master regulator of cellular mechano-transduction, *bioRxiv*. Preprint (2023 Nov 3), <https://doi.org/10.1101/2023.11.02.565386>. (Accessed 13 May 2024).
- [7] F. Kuchling, K. Friston, G. Georgiev, M. Levin, Morphogenesis as Bayesian inference: a variational approach to pattern formation and control in complex biological systems, *Phys. Life Rev.* 33 (2020) 88.
- [8] M. Levin, Bioelectric signaling: reprogrammable circuits underlying embryogenesis regeneration and cancer, *Cell* 184 (2021) 1971.
- [9] M.P. Harris, Bioelectric signaling as a unique regulator of development and regeneration, *Development* 148 (2021) dev180794.
- [10] L.F. George, E.A. Bates, Mechanisms underlying influence of bioelectricity in development, *Front. Cell Dev. Biol.* 10 (2022) 772230.
- [11] R.A. Gatenby, B.R. Frieden, Cellular information dynamics through transmembrane flow of ions, *Sci. Rep.* 7 (2017) 15075.
- [12] V. Garcia-Morales, J.A. Manzanares, S. Mafe, Weakly coupled map lattice models for multicellular patterning and collective normalization of abnormal single-cell states, *Phys. Rev. E* 95 (2017) 042324.
- [13] B. Hille, *Ion Channels of Excitable Membranes*, Sinauer Associates, Sunderland, MA, 1992.
- [14] M. Levin, The computational boundary of a “self”: developmental bioelectricity drives multicellularity and scale-free cognition, *Front. Psychol.* 10 (2019) 02688.
- [15] M. Levin, Bioelectric networks: the cognitive glue enabling evolutionary scaling from physiology to mind, *Anim. Cogn.* 26 (2023) 1865.
- [16] J. Cervera, M. Levin, S. Mafe, Bioelectricity of non-excitable cells and multicellular pattern memories: biophysical modeling, *Phys. Rep.* 1004 (2023) 1.
- [17] E. Bates, Ion channels in development and cancer, *Annu. Rev. Cell Dev. Biol.* 31 (2015) 231.
- [18] V.P. Pai, C.J. Martyniuk, K. Echeverri, S. Sundelacruz, D.L. Kaplan, M. Levin, Genome-wide analysis reveals conserved transcriptional responses downstream of resting potential change in *Xenopus* embryos, axolotl regeneration, and human mesenchymal cell differentiation, *Regeneration (Oxf)* 3 (2015) 3.
- [19] P. McMillen, R. Novak, M. Levin, Toward decoding bioelectric events in *Xenopus* embryogenesis New methodology for tracking interplay between calcium and resting potentials in vivo, *J. Mol. Biol.* 432 (2020) 605.
- [20] K. Krawczyk, S. Xue, P. Buchmann, G. Charpin-El-Hamri, P. Saxena, M.D. Hussell, J. Shao, H. Ye, M. Xie, M. Fussenegger, Electrogenetic cellular insulin release for real-time glycemic control in type 1 diabetic mice, *Science* 368 (2020) 993.
- [21] E. Sempou, V. Kostik, J. Zhu, et al., Membrane potential drives the exit from pluripotency and cell fate commitment via calcium and Mtor, *Nat. Commun.* 13 (2022) 6681.
- [22] J.R.M. Harvey, A.E. Plante, A.L. Meredith, Ion channels controlling circadian rhythms in suprachiasmatic nucleus excitability, *Physiol. Rev.* 100 (2020) 1415.

- [23] V.R. Rao, M. Perez-Neut, S. Kaja, S. Gentile, Voltage-gated ion channels in cancer cell proliferation, *Cancers* 7 (2015) 849.
- [24] A. Prindle, J. Liu, M. Asally, S. Ly, J. Garcia-Ojalvo, G.M. Süel, Ion channels enable electrical communication in bacterial communities, *Nature* 527 (2015) 59.
- [25] C.-Y. Yang, M. Bialecka-Fornal, C. Weatherwax, J.W. Larkin, A. Prindle, J. Liu, J. Garcia-Ojalvo, G.M. Süel, Encoding membrane-potential-based memory within a microbial community, *Cell Syst.* 10 (2020) 417.
- [26] R. Yuste, From the neuron doctrine to neural networks, *Nat. Rev. Neurosci.* 16 (2015) 487.
- [27] J. Cervera, S. Meseguer, S. Mafe, The interplay between genetic and bioelectrical signaling permits a spatial regionalization of membrane potentials in model multicellular ensembles, *Sci. Rep.* 6 (2016) 35201.
- [28] A. Pietak, M. Levin, Bioelectric gene and reaction networks: computational modelling of genetic, biochemical and bioelectrical dynamics in pattern regulation, *J. R. Soc. Interface* 14 (2017) 20170425.
- [29] S. Manicka, V.P. Pai, M. Levin, Information integration during bioelectric regulation of morphogenesis of the embryonic frog brain, *iScience* 26 (2023) 108398.
- [30] C.D. Tsiairis, A. Aulehla, Self-organization of embryonic genetic oscillators into spatiotemporal wave patterns, *Cell* 164 (2016) 656.
- [31] K.F. Sonnen, V.M. Lauschke, J. Uraji, H.J. Falk, Y. Petersen, M.C. Funk, M. Beaupeux, P. François, C.A. Merten, A. Aulehla, Modulation of phase shift between Wnt and Notch signaling oscillations controls mesoderm segmentation, *Cell* 172 (2018) 1079.
- [32] S. Di Talia, M. Vergassola, Waves in embryonic development, *Annu. Rev. Biophys.* 51 (2022) 327.
- [33] K. Kay, J.E. Chung, M. Sosa, J.S. Schor, M.P. Karlsson, M.C. Larkin, D.F. Liu, L. M. Frank, Constant sub-second cycling between representations of possible futures in the hippocampus, *Cell* 180 (2020) 552.
- [34] S. Bhattacharya, S.L. Brincat, M. Lundqvist, E.K. Miller, Traveling waves in the prefrontal cortex during working memory, *PLoS Comput. Biol.* 18 (2022) e1009827.
- [35] C. Fields, J. Bischof, M. Levin, Morphological coordination: a common ancestral function unifying neural and non-neural signaling, *Physiology* 35 (2020) 16.
- [36] O. Hoeller, J.E. Toettcher, H. Cai, Y. Sun, C.-H. Huang, M. Freyre, M. Zhao, P. N. Devreotes, O.D. Weiner, G β Regulates Coupling between actin oscillators for cell polarity and directional migration, *PLoS Biol.* 14 (2016) e1002381.
- [37] J. Kim, E. Winfree, Synthetic in vitro transcriptional oscillators, *Mol. Syst. Biol.* 7 (2011) 465.
- [38] H.M. McNamara, R. Salegame, Z.A. Tanoury, H. Xu, S. Begum, G. Ortiz, O. Pourque, A.E. Cohen, Bioelectrical domain walls in homogeneous tissues, *Nat. Phys.* 16 (2020) 357.
- [39] H. Ori, M. Duque, R.F. Hayward, C. Scheibner, H. Tian, G. Ortiz, V. Vitelli, A. E. Cohen, Observation of topological action potentials in engineered tissues, *Nat. Phys.* 19 (2023) 290.
- [40] J. Cervera, M. Levin, S. Mafe, Correcting instructive electric potential patterns in multicellular systems: external actions and endogenous processes, *Biophys. Biochim. A Gen. Subj.* 1867 (2023) 130440.
- [41] S. Manicka, M. Levin, Modeling somatic computation with non-neural bioelectric networks, *Sci. Rep.* 9 (2019) 18612.
- [42] P. Rühl, J.M. Langner, J. Reidel, R. Schönher, T. Hoshi, S.H. Heinemann, Monitoring of compound resting membrane potentials of cell cultures with ratemetric genetically encoded voltage indicators, *Comm. Biol.* 4 (2021) 1164.
- [43] O. Artimo, M. Grassia, M. De Domenico, J.P. Gleeson, H.A. Makse, G. Mangioni, M. Perc, F. Radicchi, Robustness and resilience of complex networks, *Nat. Rev. Phys.* 6 (2024) 114.
- [44] P. Ji, J. Ye, Y. Mu, W. Lin, P. Ji, J. Ye, Y. Mu, W. Lin, Y. Tian, C. Hens, M. Perc, Y. Tang, J. Sun, J. Kurths, Signal propagation in complex networks, *Phys. Rep.* 1017 (2023) 1.
- [45] M. Gosak, M. Milojević, M. Duh, K. Skok, M. Perc, Networks behind the morphology and structural design of living systems, *Phys. Life Rev.* 41 (2022) 1.
- [46] Y. Shui, P. Liu, H. Zhan, B. Chen, Z.-W. Wang, Molecular basis of junctional current rectification at an electrical synapse, *Sci. Adv.* 6 (2020) eabb3076.
- [47] J. Cervera, A. Alcaraz, S. Mafe, Membrane potential bi-stability in non-excitatory cells as described by inward and outward voltage-gated ion channels, *J. Phys. Chem. B* 118 (2014) 12444.
- [48] R. Law, M. Levin, Bioelectric memory: modeling resting potential bistability in amphibian embryos and mammalian cells, *Theor. Biol. Med. Model.* 12 (2015) 22.
- [49] J. Golowasch, A. Bose, Y. Guan, D. Salloum, A. Roeser, F. Nadim, A balance of outward and linear inward ionic currents is required for generation of slow-wave oscillations, *J. Neurophysiol.* 118 (2017) 1092.
- [50] O.V. Aslanidi, O.A. Mornev, O. Skyggebjerg, P. Arkhammar, O. Thastrup, M. P. Sørensen, P.L. Christiansen, K. Conradien, A.C. Scott, Excitation wave propagation as a possible mechanism for signal transmission in pancreatic islets of Langerhans, *Biophys. J.* 80 (2001) 1195.
- [51] S.R. Williams, S.R. Christensen, G.J. Stuart, M. Häusser, Membrane potential bistability is controlled by the hyperpolarization-activated current I(H) in rat cerebellar Purkinje neurons in vitro, *J. Physiol.* 539 (2002) 469.
- [52] D. Zuo, K. Chen, M. Zhou, Z. Liu, H. Chen, Kir2.1, and K2P1 channels reconstitute two levels of resting membrane potential in cardiomyocytes, *J. Physiol.* 595 (2017) 5129.
- [53] R.D. Kirkton, N. Bursac, Engineering biosynthetic excitable tissues from unexcitable cells for electrophysiological and cell therapy studies, *Nat. Commun.* 2 (2011) 300.
- [54] R.C. Stan, D.K. Bhatt, M.M. de Camargo, Cellular adaptation relies on regulatory proteins having episodic memory, *Bioessays* 42 (2020) 1900115.
- [55] J. Cervera, J.A. Manzanares, S. Mafe, Electrical coupling in ensembles of nonexcitable cells: modeling the spatial map of single cell potentials, *J. Phys. Chem. B* 119 (2015) 2968.
- [56] J. Cervera, A. Alcaraz, S. Mafe, Bioelectrical signals and ion channels in the modeling of multicellular patterns and cancer biophysics, *Sci. Rep.* 6 (2016) 20403.
- [57] J. Cervera, P. Ramirez, M. Levin, S. Mafe, Community effects allow bioelectrical reprogramming of cell membrane potentials in multicellular aggregates: model simulations, *Phys. Rev. E* 102 (2020) 052412.
- [58] V.P. Pai, J. Cervera, S. Mafe, V. Willocq, E.K. Lederer, M. Levin, HCN2 channel-induced rescue of brain teratogenesis via local and long-range bioelectric repair, *Front. Cell. Neurosci.* 14 (2020) 136.
- [59] D.S. Adams, J.M. Lemire, R.H. Kramer, M. Levin, Optogenetics in developmental biology: using light to control ion flux-dependent signals in *Xenopus* embryos, *Int. J. Dev. Biol.* 58 (2014) 851.
- [60] J.R. Lazzari-Dean, A.M.M. Gest, E.W. Miller, Measuring absolute membrane potential across space and time, *Annu. Rev. Biophys.* 50 (2021) 447.
- [61] P. Rühl, A.G. Nair, N. Gawande, S.N.C.W. Dehiwalage, L. Münster, R. Schönher, S. H. Heinemann, An ultrasensitive genetically encoded voltage indicator uncovers the electrical activity of non-excitable cells, *Adv. Sci.* 2024 (2024) 2307938.
- [62] R. Moreddu, Nanotechnology and cancer bioelectricity: bridging the gap between biology and translational medicine, *Adv. Sci.* 2023 (2024) 2304110.
- [63] T. O'Leary, A.H. Williams, A. Franci, E. Marder, Cell types network homeostasis and pathological compensation from a biologically plausible ion channel expression model, *Neuron* 82 (2014) 809.
- [64] J. Yan, A. Goldbeter, Multi-rhythmicity generated by coupling two cellular rhythms, *J. R. Soc. Interface* 16 (2019) 20180835.
- [65] J. Yan, A. Goldbeter, Robust synchronization of the cell cycle and the circadian clock through bidirectional coupling, *J. R. Soc. Interface* 16 (2019) 20190376.
- [66] F. Baluška, A.S. Reber, CBC-clock theory of life – integration of cellular circadian clocks and cellular sentience is essential for cognitive basis of life, *Bioessays* 43 (2021) e2100121.
- [67] B.T. Chernet, C. Fields, M. Levin, Long-range gap junctional signaling controls oncogene-mediated tumorigenesis in *Xenopus laevis* embryos, *Front. Physiol.* 5 (2015) 519.
- [68] S.M. Busse, P.T. McMillen, M. Levin, Cross-limb communication during *Xenopus* hindlimb regenerative response: non-local bioelectric injury signals, *Development* 145 (2018) dev164210.
- [69] M. Emmons-Bell, F. Durant, J. Hammelman, N. Bessonov, V. Volpert, J. Morokuma, K. Pinet, D.S. Adams, A. Pietak, D. Lobo, M. Levin, Gap junctional blockade stochastically induces different species-specific head anatomies in genetically wild-type Girardia dorotocephala flatworms, *Int. J. Mol. Sci.* 16 (2015) 27865.
- [70] J. Cervera, M. Levin, S. Mafe, Morphology changes induced by intercellular gap junction blocking: a reaction-diffusion mechanism, *Biosystems* 209 (2021) 104511.
- [71] C.M. Glen, T.C. McDevitt, M.L. Kemp, Dynamic intercellular transport modulates the spatial patterning of differentiation during early neural commitment, *Nat. Commun.* 9 (2018) 4111.
- [72] G. Pernelle, W. Nicola, C. Clopath, Gap junction plasticity as a mechanism to regulate network-wide oscillations, *PLoS Comput. Biol.* 14 (2018) e1006025.
- [73] F. Varela, J.P. Lachaux, E. Rodriguez, J. Martinerie, The brainweb: phase synchronization and large-scale integration, *Nat. Rev. Neurosci.* 2 (2001) 229.
- [74] B. Reid, M. Zhao, The electrical response to injury: molecular mechanisms and wound healing, *Adv. Wound Care* 3 (2014) 184.
- [75] M. Li, X. Wang, P. Rajagopalan, L. Zhang, S. Zhan, S. Huang, W. Li, X. Zeng, Q. Ye, Y. Liu, K. Zhong, J.M. Kim, J. Luo, S. Dong, R. Gu, X. Wang, W.-Q. Tan, Toward controlled electrical stimulation for wound healing based on a precision layered skin model, *ACS Appl. Bio Mater.* 3 (2020) 8901.
- [76] P.R.F. Rocha, P. Schlett, L. Schneider, M. Dröge, V. Mailänder, H.L. Gomes, P.W. M. Blom, D.M. de Leeuw, Low frequency electric current noise in glioma cell populations, *J. Mater. Chem. B* 3 (2015) 5035.
- [77] M. Ribeiro, A. Elghajji, S.P. Fraser, Z.D. Burke, D. Tosh, M.B.A. Djamgoz, P.R. F. Rocha, Human breast cancer cells demonstrate electrical excitability, *Front. Neurosci.* 14 (2020) 404.
- [78] P. Quicke, Y. Sun, M. Arias-Garcia, M. Beykou, C.D. Acker, M.B.A. Djamgoz, C. Bakal, A.J. Foust, Voltage imaging reveals the dynamic electrical signatures of human breast cancer cells, *Comm. Biol.* 5 (2022) 1178.
- [79] S.A. Newman, R. Bhat, T. Glimm, Spatial waves and temporal oscillations in vertebrate limb development, *Biosystems* 208 (2021) 104502.
- [80] L. Xiong, A. Garfinkel, Are physiological oscillations physiological? *J. Physiol.* (2024) <https://doi.org/10.1113/JP285015>.
- [81] P. Casani-Galdon, J. Garcia-Ojalvo, Signaling oscillations: molecular mechanisms and functional roles, *Curr. Opin. Cell Biol.* 78 (2022) 102130.
- [82] H.L. Gomes, R. Félix, M. Medeiros, Y. Elamine, D. Power, Extracellular bioelectrical lexicon: detecting rhythmic patterns within dermal fibroblast populations, Preprint (Version 1) available at Research Square (2023), <https://doi.org/10.21203/rs.3.rs-3286884/v1>.
- [83] K.F. Sonnen, A. Aulehla, Dynamic signal encoding-From cells to organisms, *Semin. Cell Dev. Biol.* 34 (2014) 91.
- [84] G. Pezzulo, M. Levin, Re-membering the body: applications of computational neuroscience to the top-down control of regeneration of limbs and other complex organs, *Integr. Biol.* 7 (2015) 1487.
- [85] A. Hanson, Spontaneous electrical low-frequency oscillations: a possible role in Hydra and all living systems, *Phil. Trans. R. Soc. B* 376 (2021) 20190763.
- [86] J. Macia, B. Vidiella, R.V. Solé, Synthetic associative learning in engineered multicellular consortia, *J. R. Soc. Interface* 14 (2017) 20170158.

- [87] V.P. Pai, A. Pietak, V. Willocq, B. Ye, N.Q. Shi, M. Levin, HCN2 Rescues brain defects by enforcing endogenous voltage pre-patterns, *Nat. Comm.* 9 (2018) 998.
- [88] N.C. Spitzer, Electrical activity in early neuronal development, *Nature* 444 (2006) 707.
- [89] H. Ma, H.G. Khaled, X. Wang, N.J. Mandelberg, S.M. Cohen, X. He, R.W. Tsien, Excitation-transcription coupling, neuronal gene expression and synaptic plasticity, *Nat. Rev. Neurosci.* 24 (2023) 672.
- [90] C.-H. Huang, C.-K. Lin, New biophysical rate-based modeling of long-term plasticity in mean-field neuronal population models, *Comput. Biol. Med.* 163 (2023) 107213.
- [91] M. Kojic, M. Milosevic, V. Simic, V. Geroski, A. Ziemys, N. Filipovic, M. Ferrari, Smeard multiscale finite element model for electrophysiology and ionic transport in biological tissue, *Comput. Biol. Med.* 108 (2019) 288.
- [92] S. Farashi, P. Sasaniour, H. Rafii-Tabar, Investigation of the role of ion channels in human pancreatic β -cell hubs: a mathematical modeling study, *Comput. Biol. Med.* 97 (2018) 50.
- [93] F. Sun, K.D. Poss, Inter-organ communication during tissue regeneration, *Development* 150 (2023) dev202166.
- [94] A.M. Rajnicek, N. Casan-Pastor, Wireless control of nerve growth using bipolar electrodes: a new paradigm in electrostimulation, *Biomater. Sci.* 12 (2024) 2180.

Supplemental Material:

Modeling multicellular oscillatory phenomena: the coupling between bioelectricity and transcription

Javier Cervera,¹ José A. Manzanares,¹ Michael Levin,^{2,3,4} Salvador Mafe^{1,3}

¹*Dept. Termodinàmica, Facultat de Física, Universitat de València, Burjassot, Spain*

²*Dept. of Biology, Tufts University, Medford, MA 02155*

³*Allen Discovery Center at Tufts University, Medford, MA 02155*

⁴*Wyss Institute for Biologically Inspired Engineering, Harvard University, Boston, MA 02215*

In this supplemental material, experimental examples of how instructive multicellular patterns with *depolarized* (low absolute value) and *polarized* (high absolute value) cell potential regions can allow the long-range temporal coordination of gene expression are given. Additional information concerning the biophysical model, technical details of the simulation methodology, and supplementary results are also provided.

I. MULTICELLULAR PATTERNS WITH DEPOLARIZED AND POLARIZED CELL POTENTIAL REGIONS ARE INSTRUCTIVE

Single-cell regulatory networks can be influenced by the neighboring cells in morphogenesis, regeneration, and cancer (Fig. S1).

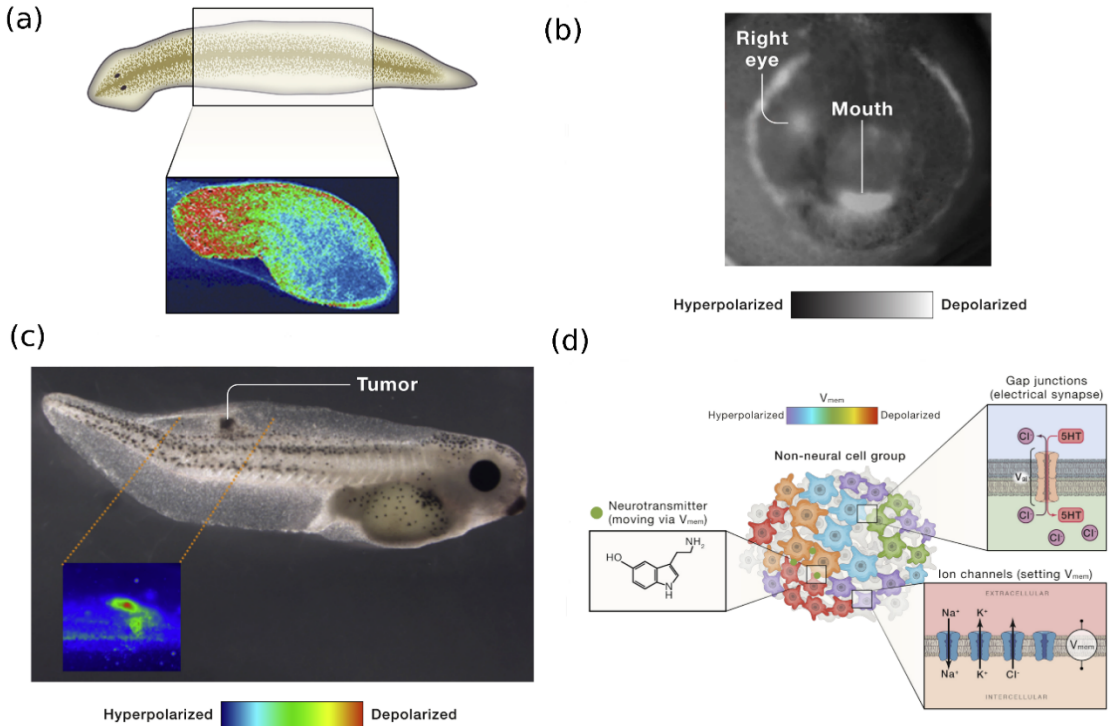


Figure S1. Depolarized and polarized regions (with low and high absolute cell potential, respectively) are characteristic of development, regeneration, and tumorigenesis. (a) Voltage-sensitive dyes show regions with similar cell polarization states (*modules*) that are instructive for the axial polarity of a flatworm. (b) The modules also act as instructive endogenous pre-patterns for face morphogenesis in an early frog ectoderm because they are coordinated with other modules to compose different mouth and eyes gene-expression regions. (c) Early tumorigenesis signals in a depolarized module of cells electrically decoupled from the polarized neighboring cells are clearly discernible in tadpoles locally injected with human oncogenes. (d) The differently polarized regions can be regarded as *bioelectric modules* that compose a biosystem-level topology reminiscent of a *pattern memory*. This instructive pattern can be externally manipulated by acting on the single-cell channel and intercellular junction proteins, which have morphological consequences because of the local feedback between bioelectrical and transcriptional processes that continuously update the cell state with time. Images taken from Ref. [1].

II. SIMULATION METHODOLOGY

The model equations and parameters used in the simulations have been explained in the *Appendix*. The numerical procedure used to conduct the simulations is now described. Additional technical details concerning the algorithms used can be found elsewhere [2]. The ensemble of cells was constructed by generating a Voronoi diagram [3] in 2D using a seed of points placed from a square grid whose position (coordinates x and y) was varied randomly within a 25% of the grid size (Fig. S2). The generated diagram provides the different regions delimiting the cells including its vertices and edges. Two neighboring cells share one edge. The final ensemble is cut off from the Voronoi diagram. Once the geometry is determined, we assign the bioelectrical parameters to every cell.

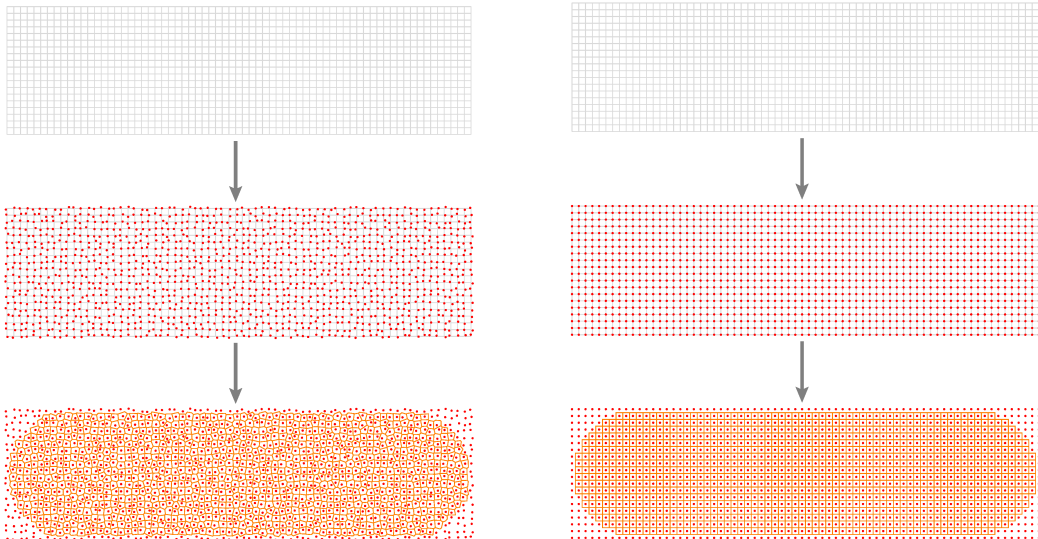


Figure S2. Construction of the cell ensemble geometry by the generation of a Voronoi diagram from a seed of points of a distorted square grid (*left*). By comparison, using a regular square grid would give a regular ensemble (*right*).

Initially, we assign the cell potential of the whole ensemble to the polarized value of the steady-state potential obtained for the single-cell, unconnected with its neighbors,

in the *right* region. This potential determines the steady-state values of the mRNA and protein concentrations. Then, the selected value of rate constant $r_{m,pol}^o$ is introduced in the cells of the *left* region and all the cells in the ensemble are connected to their neighbors by the intercellular gap junctions. The evolution of the system with time is calculated using the following finite-difference scheme.

First, a maximum time variation for the cell potential of 0.1 mV is set together with minimum and maximum time steps of $\Delta t_{\min} = 0.01$ and $\Delta t_{\max} = 1000$, respectively. Similarly, the maximum time variations of the mRNA and protein concentrations are set as the ensemble average of the initial values of m_{pol} and m_{dep} , and p_{pol} and p_{dep} divided by 100, respectively. Then, for each simulation time, the time variations of every cell potential \dot{V}_i , mRNA $\dot{m}_{pol,i}$ and $\dot{m}_{dep,i}$, and protein concentrations $\dot{p}_{pol,i}$ and $\dot{p}_{dep,i}$, are calculated from the equations of the genetic regulatory network in the main text. Because the bioelectric and transcriptional characteristic times are very different, we need an adaptative time step algorithm. In our case, the time step Δt is obtained as the minimum of those times, but keeping Δt between Δt_{\min} and Δt_{\max} time steps. Then, the time, cell potentials, mRNA concentrations, and protein concentrations are updated as $t \rightarrow t + \Delta t$, $V_i \rightarrow V_i + \Delta t \dot{V}_i$, $m_{pol,i} \rightarrow m_{pol,i} + \Delta t \dot{m}_{pol,i}$, $m_{dep,i} \rightarrow m_{dep,i} + \Delta t \dot{m}_{dep,i}$, $p_{pol,i} \rightarrow p_{pol,i} + \Delta t \dot{p}_{pol,i}$, and $p_{dep,i} \rightarrow p_{dep,i} + \Delta t \dot{p}_{dep,i}$, respectively. The calculation proceeds until the prescribed time is reached.

III. OTHER MULTICELLULAR SIMULATIONS

Fig. S3 shows the multicellular time snapshots corresponding to different simulation parameters in Fig. 4 (relative *left* region sizes of 20% and 90%) and Fig. 6

(junction conductance $G^o / G_{\text{ref}} = 0.05$). The video *Mobile Interfacial Regions* corresponds to the simulations of Fig. 7.

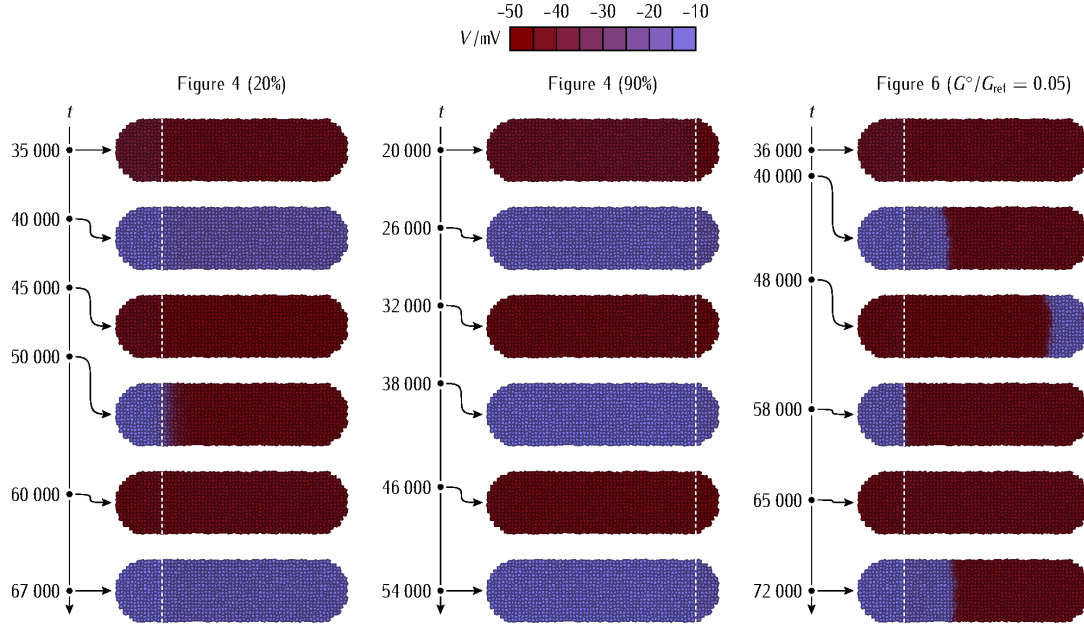


Figure S3. Multicellular time snapshots for Fig. 4 (*left* region sizes of 20% and 90%) and Fig. 6 (junction conductance $G^o / G_{\text{ref}} = 0.05$).

REFERENCES

- [1] M. Levin, Bioelectric signaling: Reprogrammable circuits underlying embryogenesis regeneration and cancer, *Cell* **184**, 1971 (2021).
- [2] J. Cervera, M. Levin, S. Mafe, Bioelectricity of non-excitable cells and multicellular pattern memories: biophysical modeling, *Phys. Rep.* **1004**, 1 (2023).
- [3] P. Virtanen, R. Gommers, T.E. Oliphant, *et al.*, SciPy 1.0: Fundamental Algorithms for Scientific Computing in Python, *Nat. Methods* **17**, 261 (2020).